Prepared for the National Institutes of Health
National Institute of Neurological Disorders and Stroke
Division of Stroke, Trauma and Neurodegenerative Disorders
Neural Prosthesis Program
Bethesda, MD 20892

Microstimulation of the Lumbosacral Spinal Cord: Mapping

NIH-NINDS-N01-NS-5-2331

Quarterly Progress Report #11

Period Covered: 1 April, 1998- 30 June, 1998

Principal Investigator: Warren M. Grill, Ph.D.[1]
Co-Investigator: Musa A. Haxhiu, M.D., Ph.D.[2]

Departments of [1]Biomedical Engineering and [2]Medicine
Case Western Reserve University
Cleveland, OH, 44106-4912

ABSTRACT

The objectives of this project are to define the anatomical locations of spinal neuronal populations involved in control of genitourinary and motor functions, and to map the physiological responses evoked in the genitourinary and hindlimb motor systems by microstimulation in the lumbosacral spinal cord. During this quarter we have made progress on both of these objectives. We continued work on co-localizing neurotransmitters and the protein product (c-Fos) of the immediate early gene c-fos to determine the location and neurochemical identity of spinal interneurons active during micturition. Quantitative results of these studies indicate that few sacral neurons co-localize c-Fos and parvalbumin, a calcium binding protein that it is marker for GABAergic neurons. We continued microstimulation studies to map the hindlimb motor responses evoked by intraspinal microstimulation, including mapping of the contralateral hemicord. The results of these experiments continue to support the hypothesis that intraspinal microstimulation can evoke two classical spinal reflexes: flexion withdrawal and crossed extension. The magnitude of these responses is limited and they accommodate rapidly. Finally, we developed a new method and to measure endpoint forces of the hindlimb throughout its workspace. This will enable us to more fully characterize the motor responses evoked by microstimulation of the lumbar spinal cord.

INTRODUCTION

Electrical stimulation of the nervous system is a means to restore function to individuals with neurological disorders. The objective of this project is to investigate the feasibility of neural prosthetics based on microstimulation of the spinal cord with penetrating electrodes. Specifically, we use chemical and viral retrograde tracers, stimulation mapping, and immediate early gene expression to determine the locations in the spinal cord of the neuronal populations that control genitourinary and motor functions in the male cat. We use selective microstimulation with penetrating activated iridium microelectrodes to determine the physiological effects of stimulation of different neural populations. The results of this project will answer fundamental questions about microstimulation of the spinal cord, and lead to development of a new generation of neural prosthetics for individuals with neurological impairments.

During the eleventh quarter of this contract we continued anatomical mapping of spinal neurons that are involved in regulation of the genitourinary system. We also measured the knee torques and muscle activity (electromyograms) evoked by microstimulation of the contralateral lumbar spinal cord. New instrumentation, which will enable us to more fully characterize the hindlimb motor responses evoked by microstimulation was designed and fabricated. Below each of our accomplishments is summarized.

PROGRESS IN THIS QUARTER

I. Anatomical Tracing of Genitourinary Innervation

Colocalization of Parvalbumin and c-fos in Sacral Spinal Neurons Involved in Regulation of Micturition

During this quarter we continued studies to determine the neurochemical identity of neurons in the sacral spinal cord. Specifically, we quantified the number of neurons which expressed c-fos, parvalbumin, or both c-fos and parvalbumin. Parvalbumin is a calcium binding protein that is found in GABAergic neurons of the central nervous system [Heizmann, 1984, Celio, 1986]. The immediate early gene c-fos enables identification of the location of neurons involved in regulation of genitourinary function, as described in previous progress reports. However, these data do not provide any information on the function of the identified neurons. As a first step in identifying

neural function we are co-localizing neurotransmitters with c-fos in genitourinary related neurons. The purpose of these experiments is to determine the location of inhibitory spinal interneurons (i.e. expressing GABA, an inhibitory transmitter with widespread distribution in the spinal cord).

METHODS

We used expression of the c-*fos* gene encoded protein c-Fos to identify sacral spinal neurons that were active during reflex micturition, and co-localization with parvalbumin (PV), a calcium binding protein present in GABAergic neurons, to identify putative inhibitory neurons. Adult male cats were anesthetized with α-chloralose and underwent a 1-2 h period of isometric micturition induced by ligating the proximal urethra and infusing saline into the bladder (1 ml/min) until spontaneous periodic bladder contractions occurred. Animals were perfused 1-2 h after the cessation of the stimulus, and double labeling was used to define co-expression of c-Fos with PV or GABA.

Sections of the sacral spinal cord taken from animals which had undergone 2 hours of isometric micturition were double-processed using immunohistochemistry to detect the presence of c-Fos and GABA by detection of parvalbumin. The free floating sections were washed in PBS containing 0.3% Triton-X and then exposed for 30 min to PBS-Triton solution containing 3% normal rabbit serum to block non-specific binding sites. After a further wash, the tissue was placed overnight at room temperature in a primary polyclonal antibody solution (1:10,000 dilution of rabbit anti-Fos (Ab-5) in PBS; Oncogene, Cambridge, MA). The sections were rinsed, incubated with biotinylated goat anti-rabbit secondary antiserum and further processed using the standard biotin avidin-peroxidase kit (ABC-elite kit; Vector Labs, Burlingame, CA). The immunoreaction was visualized by incubating the sections with 0.02% 3.3'-diaminobenzidine containing 0.01% hydrogen peroxide for 6 min. A purple-black reaction product was obtained by adding nickel chloride to the peroxidase reaction (40 ml of 8% $NiCl_2$ solution per 100 ml of DAB solution). Thereafter, sections were incubated for 16 hours in a solution containing monoclonal antibody formed in mouse (1:2,000 mouse anti-parvalbumin (PARV-19) in PBS; Sigma, St. Louis, MO). The sections were washed in PBS (2x), incubated for four hours with biotinylated goat anti-mouse secondary antiserum, and further processed using the standard biotin avidin-peroxidase kit (ABC-elite kit; Vector Labs, Burlingame, CA). Parvalbumin immunoreactivity was visualized by the peroxidase reaction omitting the $NiCl_2$ addition to DAB to obtain a brown reaction product.

Slides were viewed using bright-field microscopy and locations of cells exhibiting immunoreactivity to c-Fos or parvalbumin (PV) described according to the conventions of Rexed [1954]. High resolution, low magnification prints were made of 3 sections from the S2 sacral segment in each of three animals. The printouts were used to mark Fos-positive and/or PV-positive cells identified under higher magnifications views of the same sections. All cell counts were made by an investigator blinded to the procedure conducted on the animal

RESULTS

Co-localization of Fos-immunoreactivity with parvalbumin-immunoreactivity was identified by viewing the sections under bright field. The contrasting immunoprecipitates were readily distinguishable. Immunostaining for Fos protein was exclusively nuclear, and immunoreactive nuclei were seen as dark, round or oval structures. Immunoprecipitate indicating parvalbumin immunoreactivity was confined to the cytoplasm (see fig. 9.3, QPR 11). Parvalbumin (PV) containing cells were observed in the sacral spinal cord in regions where Fos-containing cells were also found including around the central canal and within the intermediolateral region.

Operated unstimulated controls exhibited few neurons expressing c-Fos which were localized to the superficial dorsal horn (laminae I and II). Further, omission of the primary or secondary antibodies resulted in absence of labeling, demonstrating that no false positive results were obtained with these reagents.

In stimulated animals, neurons expressing c-Fos were found bilaterally in S1-S3 and were localized to the lateral portion of the superficial dorsal horn (laminae I and II), the intermediolateral region (lateral laminae V-VII), and around the central canal (lamina X and medial laminae V-VII).

The number of neurons expressing only c-Fos immunoreactivity (463), only PV immunoreactivity (119), or immunoreactivity for both c-Fos and PV (25) were counted in 3 sections from each of 3 animals. Within the three regions where neurons exhibiting c-Fos immunoreactivity were identified, only 25/463 cells (5%) also expressed PV (fig. 11.1). Cells co-localizing both PV and c-Fos were found mostly around the central canal with fewer double labeled cells in the intermediolateral region, and none in the dorsal horn. These results indicate that a relatively small sub-population of neurons activated during reflex micturition express GABAergic traits.
These results are somewhat surprising because previous results indicate that neurons around the central canal in the sacral cord, that receive descending input from Barrington's nucleus, contain the inhibitory neurotransmitter GABA [Blok and Holstege, 1997]. Furthermore, external urethral sphincter motoneurons are contacted by GABAergic terminals [Ramirez-Leon and Ulfhake, 1993, Ramirez-Leon et al., 1994]. Therefore, we expected to find GABA co-localized with c-fos in some spinal neurons active during micturition. Such cells may function to inhibit somatic motoneurons leading to a reduction in urethral pressure during micturition. However, while all parvalbumin-positive neurons are also GABAergic, not all GABAergic neurons are parvalbumin positive [Cowan et al., 1990]. Therefore, our result must be confirmed with a more specific antibody such as anti-GABA or anti-GAD (glutamate decarboxylase, a GABA precursor).

II. Microstimulation of the Lumbar Spinal Cord in Male Cats

The objective of these experiments is to determine the physiological effects in the motor system of microstimulation of neuronal populations in the spinal cord. The specific focus of current work was to measure the hindlimb motor responses (knee torque, intramuscular electromyograms) produced by microstimulation of the lumbosacral spinal cord at the L6/L7 border and to evaluate the recruitment properties of torques evoked by microstimulation.

Methods

Male cats were anesthetized with ketamine HCl (15-20 mg/kg, IM), and a venous catheter was inserted in the cephalic vein. Anesthesia was maintained with α-chloralose (60 mg/kg IV, supplemented at 15 mg/kg). A laminectomy was made to remove the L4-L7 vertebrae. The animal was mounted in a spinal frame with pins at the hips, the head in a headholder, and vertebral clamps at L3 and S1. Body temperature was maintained between 37° and 39° C with a thermostatically controlled heat lamp, warm 5% dextrose saline with 8.4 mg/cc sodium bicarbonate added was administered IV (~20 cc/hr), and heart rate was monitored throughout the experiment. Dexamethasone (2 mg/kg, IV) was administered at the completion of the laminectomy and every 6 hours thereafter to prevent inflammation of the spinal cord.

The torques generated about the knee were measured using a custom-built strain gage instrumented beam (described in QPR #2). Torque signals were amplified, low pass filtered (fc=100 Hz), and sampled by computer (fs=200Hz). Torques were quantified by taking the peak torque and the average torque during the stimulus train.

Intramuscular bipolar fine wires (stainless steel wires, 0.0018" diameter, insulated except for 2 mm at their tips) were used to record electromyograms from 4 hindlimb muscles: semimembranosus, biceps femoris, vastus medialis, and vastus lateralis. EMG signals were amplified, filtered (10 Hz-1 kHz), and sampled (2.5 kHz). Off-line, EMG signals were rectified, integrated, and the final value of the integral was used to quantify the EMG response. For each muscle, the magnitude of the rectified integrated EMG was normalized to the maximum response obtained from that muscle.

Stimulation was accomplished with activated iridium microwire electrodes (50μm Epoxylite insulated iridium wire with an exposed electrochemically determined surface area of ~225 μm^2 and a 1 μm tip, HMRI IS300, Huntington Medical Research Institutes, Pasadena, CA). Stimuli were charge balanced biphasic pulses with an amplitude of 10-150μA and a pulsewidth of 100 μs applied as 1 s to 100 s continuous trains with a frequency between 2 Hz and 100 Hz. The standard mapping stimulus was a 1 s 20 Hz train of 100 μA 100 μs pulses. Vertical, dorsal-to-ventral

penetrations (increment=100-400 μm) were made at multiple mediolateral locations (increment=250 μm in the middle of the lumbar segments and at intersegmental boundaries.

Results

The spatial mapping conducted during this quarter provided further data to support that the structure of maps is repeatable across animals, that mapping results parallel previous results with retrograde anatomical tracing, and that there are reproducible differences in the structure of the maps along the rostrocaudal axis.

The maps generated during this quarter continue to support the hypothesis that two classical spinal reflexes, flexion withdrawal and crossed extension, can be evoked by intraspinal microstimulation. Maps of the isometric knee torque evoked in the right hindlimb by microstimulation at the level of the border between the L5 and L6 segments are shown in fig. 11.2. The maps show the peak (A) and average (B) torques evoked by 1 s 20 Hz trains of 100 μs 100 μA pulses, plotted in greyscale values, over a spatial plot of the cord where the midline is at mediolateral 0 and the dorsal surface is at the top. To improve the scaling only the dorsal half of the cord is shown, although the ventral aspect was also mapped. Stimulation in the ipsilateral dorsal aspect of the cord, in the region of the dorsal root entry zone (black asterisk), produced flexion torques (fig. 11.2). The responses had a strong onset followed by a rapid decay, and thus the peak torque was much larger than the average torque (compare A and B in fig. 11.2). Microstimulation in the contralateral dorsal horn, also in the region of the dorsal root entry zone (white asterisk), produced extension torques. Like the flexion torques produced by dorsal ipsilateral stimulation, these responses had a strong onset followed by a rapid decay, and thus the peak torque was much larger than the average torque (compare A and Bin fig. 11.2).

As seen when comparing the two maps in fig. 11.2, the peak torques were much larger than the average torques. The responses to stimulation in the dorsal aspect of the cord had a strong onset followed by a rapid decay, and this was observed at all frequencies examined, from 2 Hz to 40 Hz. The extension and flexion torques produced by stimulation at dorsal locations (asterisks in fig. 11.2) with a range of stimulus frequencies are shown in fig. 11.3 A and B, respectively. For comparison, a flexion response evoked in a ventral location in shown in fig. 11.3 C. Frequencies from 2 Hz to 40 Hz were tested and the duration of the stimulus train was adjusted at each frequency to deliver the same total number of pulses. Also shown are the responses obtained with the standard mapping stimulus (20 Hz, 1 s) before and after different frequencies were tested. These data (a and g in A and B) demonstrate that the responses were stable in time. The response was similar at all tested frequencies and was characterized by a rapid onset and immediate decay. In some cases (Ab, Ac, Bb), lower frequency stimulus trains evoked multiple responses, but the amplitude of subsequent response was smaller in all cases than the initial response.

These data suggest that microstimulation in the dorsal aspect of the spinal cord evokes two classical spinal reflexes: ipsilateral flexion withdrawal and contralateral (crossed) extension. However, the magnitude of the responses is small and not sustained during the stimulus train.

III. Instrumentation for Measuring Hindlimb Motor Responses to Intraspinal Microstimulation

A new apparatus was designed and constructed to allow for a fuller characterization of the hindlimb motor responses produced by intraspinal microstimulation. In the new configuration, forces at the paw are recorded via a six-axis commercial force transducer (Nano-25 from ATI Industrial Automation, Peachtree Center, 503-D Highway 70 East, Garner, NC 27529; (919)772-0115), rather than recording torque at a single joint. These endpoint forces are then used to calculate the respective joint torques.

Theory

The angles and moments at both knee and ankle (fig. 11.4) can be determined from simple inverse kinematics. By carefully determining link lengths and the hip center of rotation (via X-rays), the knee and ankle angles are reconstructed by:

$\theta_k = a\tan 2(y_S, x_S) - a\tan 2(\kappa, x_S^2 + y_S^2 + l_a^2 - l_k^2)$ [1], for the knee angle and

$\theta_a = \theta_k + a\tan 2(\kappa, x_S^2 + y_S^2 - l_k^2 - l_a^2)$ [2], for the ankle angle, both in radians. With

$\kappa = \sqrt{(x_S^2 + y_S^2 + l_a^2 + l_k^2)^2 - 2[(x_S^2 + y_S^2)^2 + l_a^4 + l_k^4]}$ [3].

Where (x_S, y_S) is the sensor position relative to the knee joint, l_k is the lower leg length, l_a is the paw length (from the ankle to sensor's z-axis). Assuming links lengths in the 10-12 cm range, and with length measurement errors in the 2 mm range (i.e. greater than the 1 mm error expected from our planned X-ray measurements), the resulting errors in the joint angles are within 2°-3°, which is more than adequate.

Torques at the knee and ankle can then be calculated using the Jacobian of the 2D linkage formed by the paw and lower leg, and the end-point measured forces. Torques are simply obtained by $\tau = J^t F$. From the form of the transpose of the Jacobian:

$$J^T = \begin{bmatrix} -l_k \sin\theta_k - l_a \sin\theta_a & l_k \sin\theta_k + l_a \sin\theta_a \\ -l_a \sin\theta_a & l_a \cos\theta_a \end{bmatrix}, \quad [4]$$

where l_k and l_a are the lower leg and paw lengths respectively, and θ_k and θ_a are the knee and ankle joint angles (in absolute angles). One can see how errors in the measurements of segments lengths are directly reflected in the torques estimates, while errors in the joint angles measurements are reflected through a nonlinear function (sine and cosine) that reduces the effects of measurement error (a 10% change in angle does not translate in a 10% change in torque). We plan on reducing segment length errors to within 1 mm by taking X-rays of the limb, which will ensure that joint angles errors are within 3°. Since torque measurements are in almost every cases obtained via measurement of some deflection that is sensitive to where force is applied, the proposed methodology is expected to be as accurate as a direct measurement of torques.

Since the new apparatus allows us to position the sensor in the sagittal plane of the cat's hindlimb, we will be able to characterize the action of electrical stimulation at various locations throughout the workspace of the limb.

Positioner Assembly

The positioner was assembled from three 12" slides obtained from Edmund Scientific (part number A31,241; Edmund Scientific Company, 101 East Gloucester Pike, Barrington, NJ 08007-1380; (609)573-6250). A drawing of the assembly is provided in figure 11.5. Two of the rails form the vertical axis, while the third rail (mounted on the carrier of the two vertical axes) forms the horizontal axis. The carriers are mounted on a dovetail fit on the rail, and move along the rail via a rack-and-pinion mechanism. A scale is mounted on the rail and allows repeatable positioning of the carrier. The sensor's workspace is approximately 25 cm×25 cm, which covers the cat's workspace.

The force sensor mounts on the carrier of the horizontal axis, with its X-axis aligned with the horizontal (rostrocaudal axis of the cat), the Y-axis with the vertical (cat's dorsoventral axis) and the Z-axis with the transverse horizontal (cat's mediolateral axis). The force sensor is 17 mm in diameter, and 14.5 mm in height. The sensor is attached on a plate mounted on the carrier see *FORCE SENSOR ATTACHMENT PLATE* drawing (figure 11.6).

The cat's paw is rigidly attached to a plate via tie-wraps, and a small cast. The plate is mounted to the force sensor via a gimbals that allows rotation around the z-axis (see *FORCE SENSOR ATTACHMENT* drawing, figure 11.7). This allows the ankle to rotate as the end-point is moved through the various positions at which forces are measured.

Software

Our previous data collection software has been modified to allow for the display of the six forces and moments, as well as 8 channels of electromyographic activity (EMG). In addition, the software displays the forces vector collected (in the sagittal plane) allowing us to verify the structure of the forces at the paw as they are collected. As previously, the data collection is written in LabView 4.1™ (National Instruments, 6504 Bridge Point Parkway, Austin, TX 78730-5039; (512)794-0100) for the Macintosh.

Force patterns at the paw will be analyzed in the z plane (the sagittal plane of the cat). Forces will be measured on a grid covering the workspace (6 cm by 6 cm, around a central location corresponding to the leg in mid-stance), and a field will be interpolated from these measurements by dividing the grid into triangles, and interpolating the force vector inside the triangle from the corner measurements, i.e.

$$\mathbf{F}_x = a_{1,1}x+a_{1,2}y+a_{1,3},$$
$$\mathbf{F}_y = a_{2,1}x+a_{2,2}y+a_{2,3}. \qquad [5]$$

The six parameters, $a_{i,j}$, are estimated by equating the forces measured at the corners of the triangles to the $\mathbf{F}_x$, $\mathbf{F}_y$ given by the previous equations, where x and y were equal to the spatial locations of the triangle's corners (yielding six unknowns and six equations). (from [Giszter et al.; 1993]).

The software necessary for this analysis is already in place, and consists of a series of macros for the Igor application from WaveMetrics Inc. (P.O. Box 2088, Lake Oswego, OR 97035; (503)620-3001).

Parts List:

Assembly	Part Description & Number	Source
Force Sensor Attachment - Bearing assembly	ABEC-5 Bearing 7804K26	McMaster-Carr Supply (330)995-5500
Positioner Assembly	12" slides A31,241	Edmund Scientific Cie (609)573-6250

PUBLICATIONS

The following abstracts, reporting work conducted under the contract, were submitted during this quarter.

Grill, W.M., S. Hadziefendic, B.O. Erokwu, M.A. Haxhiu (1998) Co-localization of parvalbumin and c-fos in sacral spinal neurons involved in regulation of micturition. Society for Neuroscience Abstracts 24.

Grill, W.M., B. Wang, N. Bhadra, M.A. Haxhiu (1998) Spinal neurons regulating micturition: identification and effects of stimulation. 3rd Conf. Int. Functional Electrical Stimulation Soc.

OBJECTIVES FOR THE NEXT QUARTER

I. Anatomical Tracing of the Genitourinary and Hindlimb Motor Systems. We will continue our co-localization studies to identify the neurotransmitters present in neurons active during reflex

micturition. We will continue studies using spinally injected retrograde tracers to map the location and rostrocaudal extent of last order interneurons that project to spinal motoneuron pools.

II. Microstimulation of the Lumbosacral Spinal Cord: We will focus on completing analysis of data from motor system mapping studies and prepare a manuscript reporting these results. We will also undertake experiments with our new apparatus to measure the endpoint forces evoked by intraspinal stimulation.

LITERATURE CITED

Blok, B.F.M., G. Holstege (1997) On the role of the sacral intermediomedial cell column in micturition. Neuroscience Abs. 23:1521.

Celio, M.R. (1986) Parvalbumin in most gamma-aminobutyric acid containing neurons of the rat cerebral cortex. Science 231:995-997.

Cowan, R.L., C.J. Wilson, P.C. Emson, C.W. Heizman (1990) Parvalbumin-containing GABAergic interneurons in the rat neostriatum. J. Comp. Neurol. 302:197-205.

Giszter, SF, Mussa-Ivaldi, FA, and E. Bizzi. Convergent force fields organized in the frog's spinal cord, The Journal of Neuroscience, 1993, 13(2):467-491.

Heizmann, C.W. (1984) Parvalbumin, an intracellular calcium binding protien: distribution, properties, and possible roles in mammalian cells. Experientia 40:910-921.

Hsu, S.-M., L. Raine, H. Fanger (1981) Use of avidin-biotin-peroxidase complex (ABC) in immunoperoxidase techniques: A comparison between ABC, and unlabeled antibody (PAP) procedures. J. Histochem. Cytochem. 29:577-580.

Ramirez-Leon, V., B. Ulfhake (1993) GABA-like immunoreactive innervation and dendro-dendritic contacts in the ventrolateral dendritic bundle in the cat S1 spinal cord segment: an electron microscopic study. Exp. Brain Res. 97:1-12.

Ramirez-Leon, V., B. Ulfhake, U. Arvidsson, A.A. Verhofstad, T.J. Visser, T. Hokfelt (1994) Serotoninergic, peptidergic and GABAergic innervation of the ventrolateral and dorsolateral motor nuclei in the cat S1/S2 segments: an immunofluorescence study. J Chem. Neuroanat. 7:87-103.

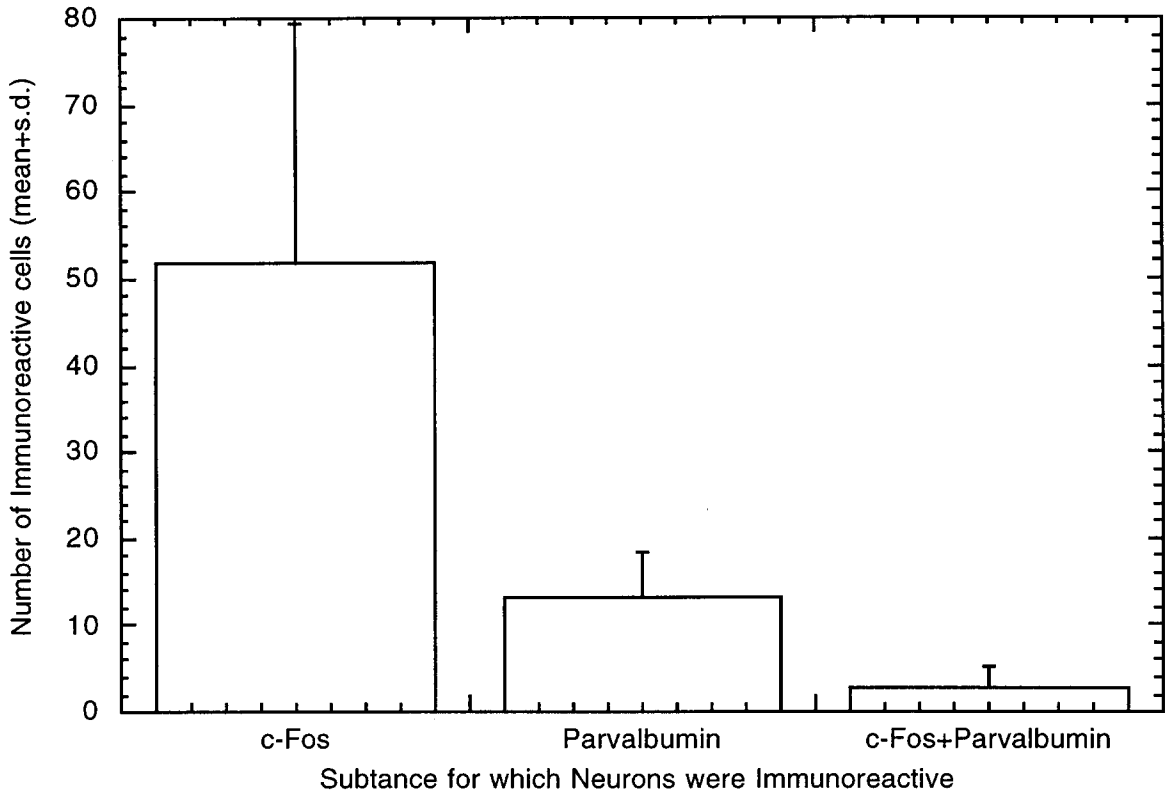

Figure 11.1 Colocalization of c-Fos and parvalbumin in sacral spinal neurons. Counts [mean ± s.d., n=9 (3 sections in each of three animal)] of the numbers of neurons expressing each substances.

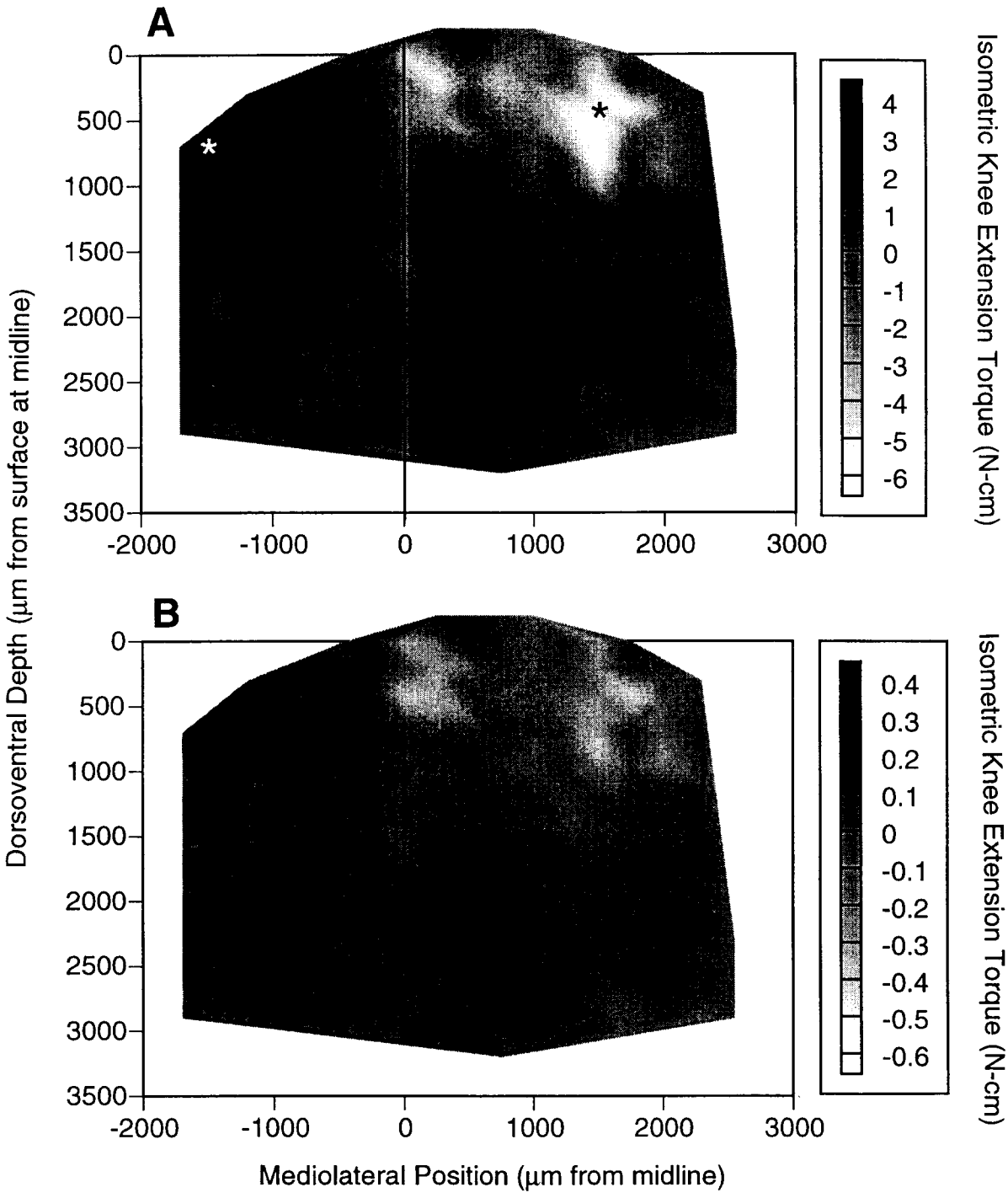

Figure 11.2 Maps of the peak (A) and average (B) isometric knee torques evoked by microstimulation of the lumbosacral (L5/6 border) spinal cord.

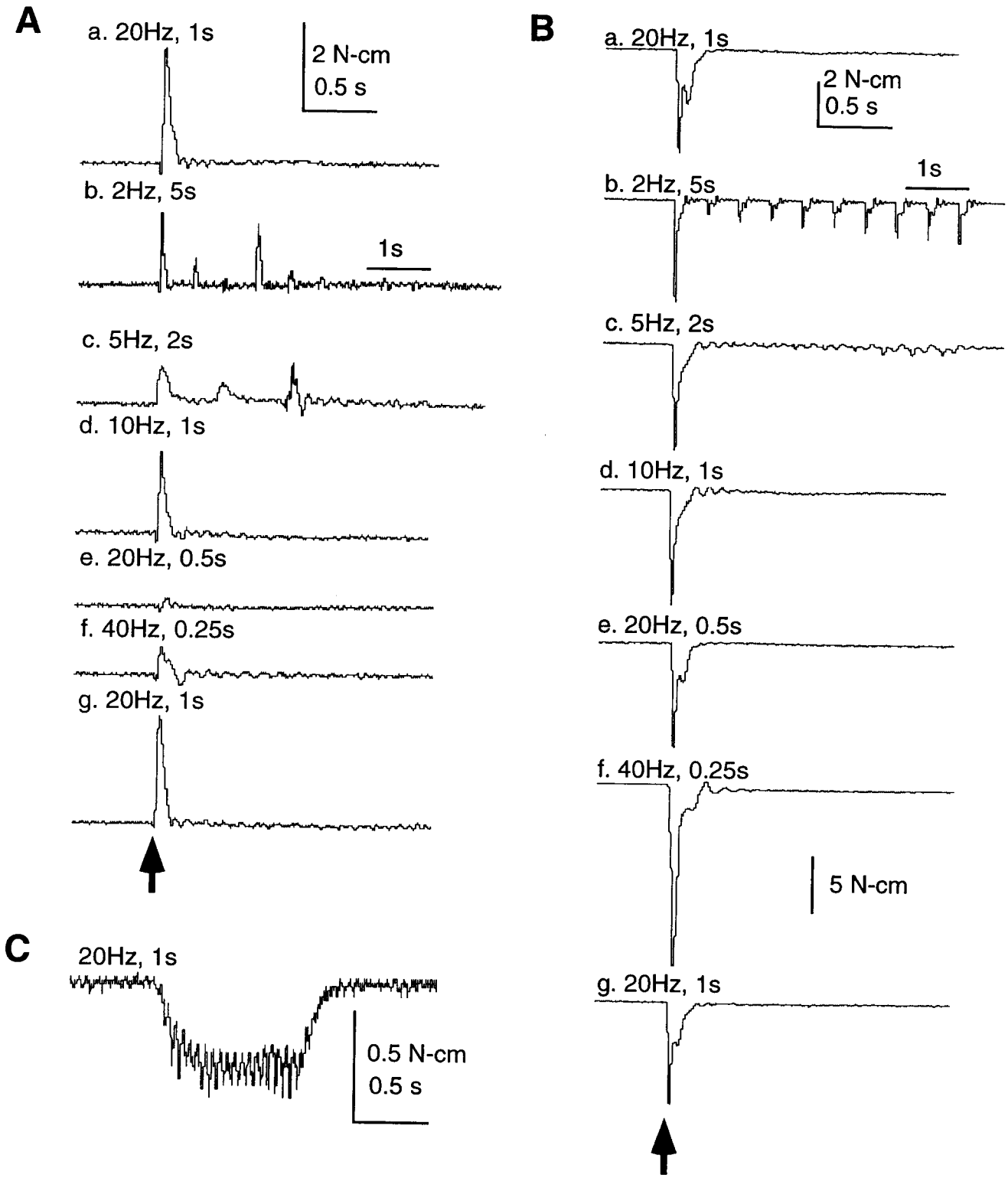

Figure 11.3 Influence of stimulus frequency on the torques evoked by stimulation in contralateral dorsal cord (A, location shown by white asterisk in fig. 11.2), ipsilateral dorsal cord (B, location shown by black asterisk in fig. 11.2), and ventral spinal cord C.

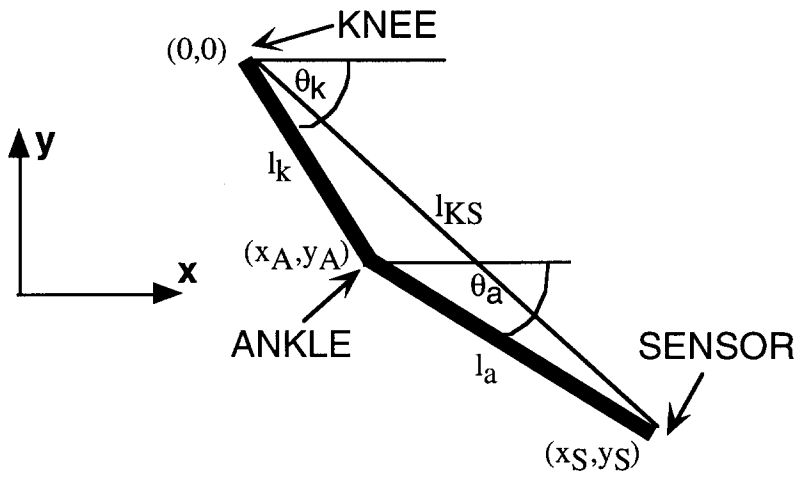

Figure 11.4. Schematic of the lower leg and paw. With the hip joint fixed, the upper leg is fixed and hence the knee position is fixed. Knee and ankle rotation angles in the sagittal plane can then be reconstructed using equations [1], [2], [3] (in the text).

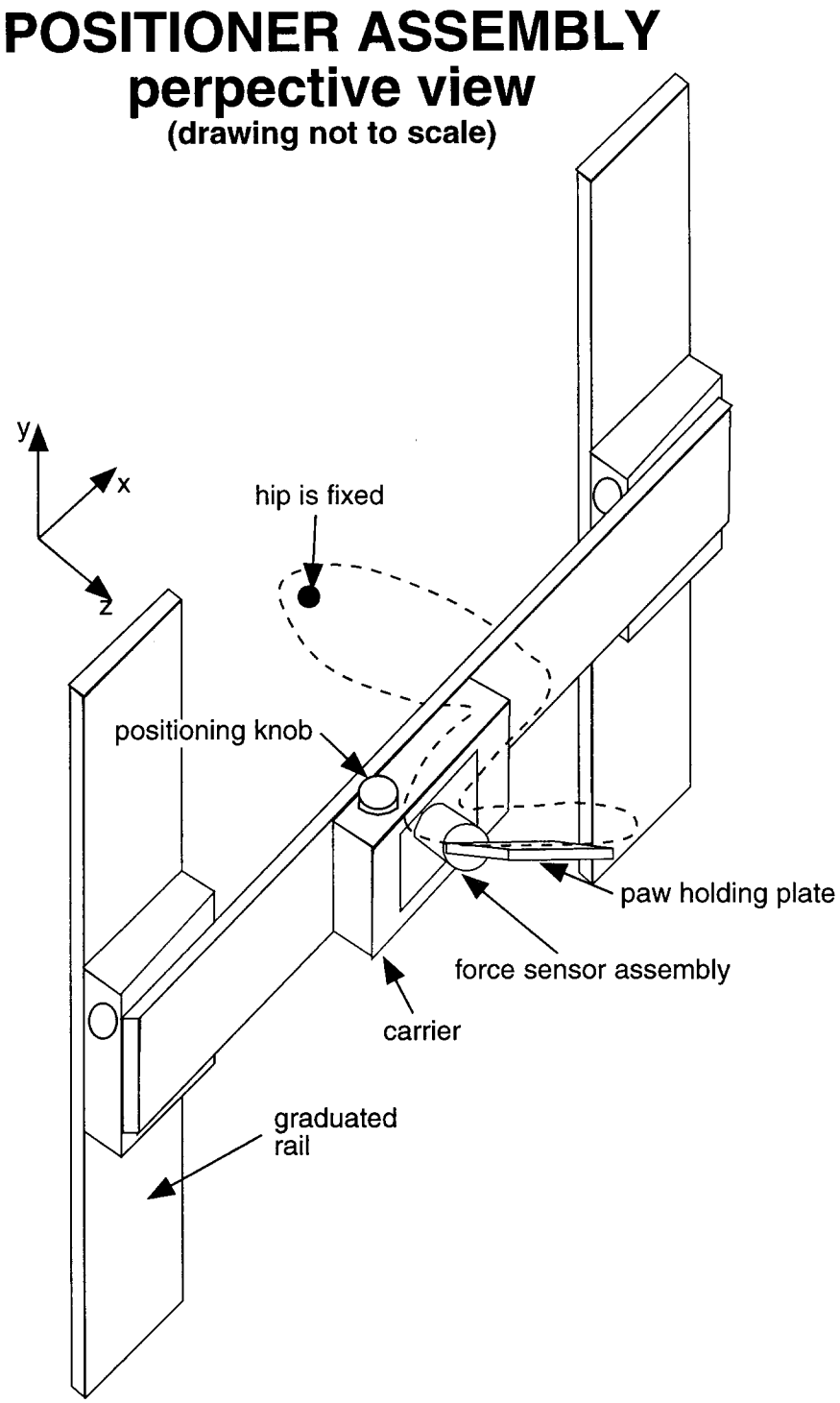

Figure 11.5: Positioner assembly drawing. The drawing gives a perspective of the set-up with the cat's hindlimb attached to the paw holding plate. The force sensor is moved along the x and y axes via rack-and-pinion mechanisms controlled by knobs on the three carriers; graduated scales on each of the rail allow for repeatable positioning.

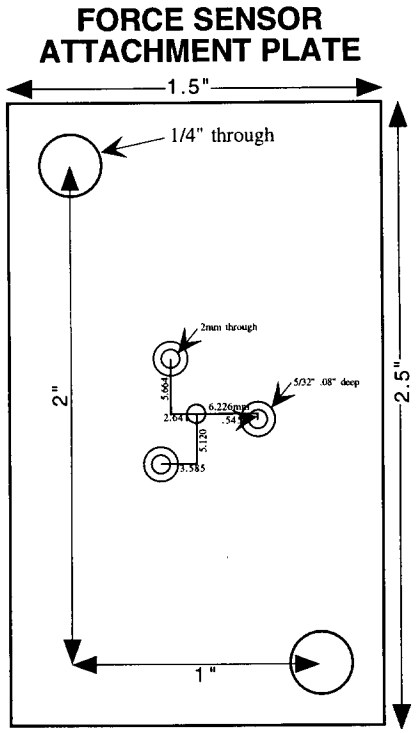

Figure 11.6: Force sensor attachment plate drawing. The force sensor is mounted on this plate via three M2-.40 screws, and the plate mounts on the carrier moving along the x axis (see Figure 2). The force sensor (Nano-25 from ATI Industrial Automation) itself is a 14.5 mm tall cylinder with a 17 mm diameter.

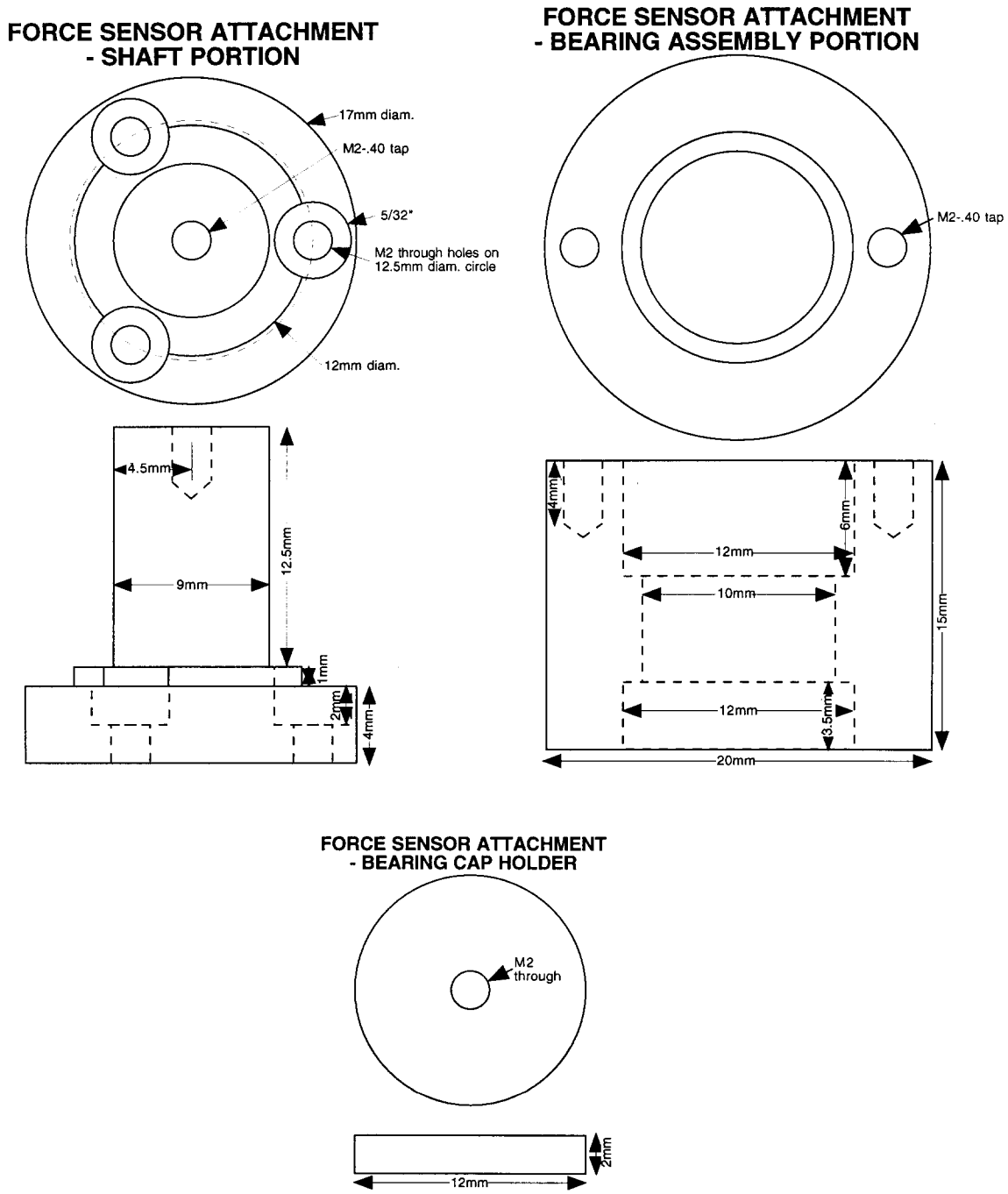

Figure 11.7. Force sensor attachment drawing. The shaft is mounted on the tool side of the force sensor, and the bearing assembly mounts on the shaft and is held in place by the cap holder. The assembly allows the ankle to rotate as the limb is moved through the workspace.